American Journal of Modern Energy
2026, Vol. 12, No. 3, pp. 42–48
https://doi.org/10.11648/j.ajme.20261203.11

SciencePG
Science Publishing Group

Research Article

Sustainable Porous Carbon from Ziziphus Fruit Waste for High Specific Capacity Electrode Materials

Hamouda Adam Hamouda[1, *], Inaam Ali Salim[2], Abdelwahab Abuelgasim Mohammed Adam[1], Taysir Abdrhman Musa[1], Elsadig Omer Fadul[3]

[1]Department of Chemistry, University of Kordofan, El Obeid, Sudan

[2]Department of Science and Technology, University of Hafr Al Batin (UHB), Nairiyah, Saudi Arabia

[3]Department of Physics, University of Kordofan, El Obeid, Sudan

Abstract

The growing demand for efficient energy storage for renewable systems requires low-cost, high-performance electrode materials. Supercapacitors offer fast charge-discharge but suffer from low energy density. Biomass-derived porous carbon is a sustainable alternative to commercial activated carbon. This study aims to synthesize hierarchical N,O-doped porous carbon from Ziziphus spina-christi fruit waste in order to evaluate the effect of alkali agent and activation time on porosity and supercapacitor performance. The carbon was prepared via carbonization at 600 ℃ followed by chemical activation with KOH or NaOH at 800 ℃ for 2 h and 3 h. The materials were characterized by FE-SEM, XRD, Raman, and N_2 adsorption-desorption. The electrochemical tests were conducted in 3-electrode system. The optimized ZSCFC-3h-KOH exhibited a high specific surface area of 917.5 m^2 g^{-1}, a hierarchical micro-mesoporous structure, and an ID/IG ratio of 0.98. In a 3-electrode system, it delivered a specific capacitance of 231.6 F g^{-1} at 1 A g^{-1} with an IR drop of only 0.03 V. The electrode showed excellent stability, retaining 94.3% of its capacitance after 10,000 cycles at 5 A g^{-1}. Z. spina-christi fruit waste is a viable, sustainable precursor for high-capacitance supercapacitor electrodes. KOH activation for 3 h is optimal for creating accessible pore networks for ion storage.

Keywords

Ziziphus Spina-christi, Biomass-derived Carbon, KOH Activation, Porous Carbon, Specific Capacity

1. Introduction

The accelerating deployment of renewable energy systems and the rapid growth of the electric vehicle market have significantly increased the demand for efficient, reliable, and cost-effective energy storage technologies [1-3]. Among various energy storage devices, supercapacitors have attracted considerable attention due to their exceptional power density, ultra-fast charge-discharge capability, long cycle life exceeding 10,000 cycles, and minimal maintenance requirements [4, 5]. However, their widespread commercial adoption remains limited by their relatively low energy density compared to lithium-ion batteries. Consequently, enhancing the electrochemical performance of supercapacitors primarily relies on

*Correspondence: Hamouda Adam Hamouda (hamoudaadam84@gmail.com)

Received: 23 June 2026; **Accepted:** 6 July 2026; **Published:** 24 July 2026

the development of advanced electrode materials that possess a large ion-accessible surface area, hierarchical porosity, and rapid ion transport pathways [6-9]. So that converting agricultural waste into porous carbon addresses both environmental concerns and material costs [10]. The biomass precursors inherently contain heteroatoms and fibrous structures that promote the development of interconnected pore networks during the thermal processing [11, 12]. The final carbon architecture, along with the activating agent and activation duration, directly influences ion diffusion and charge storage [13]. So that the chemical activation using alkaline agents such as KOH and NaOH is widely preferable because it produces carbons with highly developed microporosity and large surface area under milder conditions than the physical activation [14]. The ziziphus spina-christi fruit waste is abundantly available in Sudan and other arid regions [15]. Its lignocellulosic composition provides a natural scaffold for porous carbon formation [16, 17]. Despite this potential, the Z. spina-christi residue remains underexplored as a precursor for supercapacitor electrode. Nevertheless, the effect of alkali activation time on its porosity has not been fully clarified [18]. Motivated by these gaps, this work reports the fabrication of hierarchical N,O-doped porous carbons derived from Z. spina-christi fruit waste via a two-step process of carbonization followed by chemical activation with KOH or NaOH for 2 h and 3 h. The effect of the activating agent and activation time on the morphology, textural properties, and capacitive performance was systematically investigated [19]. The optimized carbon, ZSCFC-3h-KOH, achieved a specific surface area of 917.5 m^2 g^{-1} and delivered superior capacitance and cycling stability in a symmetric supercapacitor. These results confirm that Z. spina-christi fruit waste is a viable, sustainable precursor for high-performance supercapacitor electrodes [20].

2. Experimental

2.1. Materials

Ziziphus spina-christi fruits were collected from the El-Obied region, Kordofan State, Sudan. It was used as the biomass precursor without further pretreatment. The potassium hydroxide (KOH, 85%, Sinopharm Chemical Reagent Co., Ltd., China) and sodium hydroxide pellets (NaOH, 96%, Aladdin Co., Ltd., China) were used as chemical activating agents. The hydrochloric acid (HCl, 37%, Aladdin Ltd., Shanghai, China) was employed for post-activation washing. Polyvinylidene fluoride (PVDF, Aladdin Ltd., Shanghai, China) and carbon black (CB, Aladdin Ltd., Shanghai, China) served as binder and conductive additive, respectively. N-methyl-2-pyrrolidone (NMP, Aladdin Ltd., Shanghai, China) was used as the solvent for slurry preparation. Nickel foam (NF, 110 PPI, Aladdin Ltd., Shanghai, China) was used as the current collector. All reagents were analytical grade and used as received without additional purification.

2.2. Preparation of Ziziphus Spina-christi Fruit-derived Porous Carbon (ZSCFC)

Z. spina-christi fruits were cut into small pieces of ~1-2 cm^3, washed repeatedly with distilled water and ethanol to remove impurities, and dried at 60 ℃ for 18 h. The dried biomass was carbonized in a tube furnace at 600 ℃ for 2 h under N_2 flow with a heating rate of 5 ℃ min^{-1}. The resulting char was ground into powder. For the chemical activation, the carbon powder was physically mixed with KOH or NaOH at a mass ratio of 1: 3 [21]. The mixture was activated at 800 ℃ for 2 h or 3 h under N_2 atmosphere using the same heating rate of 5 ℃ min^{-1}. After cooling to room temperature, the activated product was washed sequentially with diluted HCl and distilled water until the filtrate reached pH 7, so as to remove residual alkali and inorganic salts. Finally, the sample was dried at 80 ℃ overnight. In this study four samples were prepared under different activation conditions and labeled as follows: ZSCFC-2h-KOH: activated with KOH for 2 h, ZSCFC-3h-KOH: activated with KOH for 3 h, ZSCFC-2h-NaOH: activated with NaOH for 2 h, ZSCFC-3h-NaOH: activated with NaOH for 3 h. The sample showing the highest surface area and capacitance, therefore, was selected for symmetric supercapacitor fabrication.

2.3. Materials Characterizations

The morphology and microstructure of the ZSCFC samples were examined by field-emission scanning electron microscopy (FE-SEM, Zeiss Ultra Plus, Germany) operated at 5 kV. Transmission electron microscopy (TEM, JEOL JEM-2100, Japan) was used to analyze the pore structure and lattice fringes. The crystal structure was determined by X-ray diffraction (XRD, Rigaku D/Max-2500, Japan) using Cu Kα radiation (λ = 1.5406 Å) in the 2θ range of 10-80 °. Raman spectroscopy was performed on a Renishaw inVia spectrometer with a 514 nm Ar^+ laser to evaluate the degree of graphitization. The specific surface area and pore size distribution were measured by N_2 adsorption-desorption isotherms at 77 K using a Micromeritics ASAP 2460 analyzer, USA. All samples were degassed at 200 ℃ for 6 h under vacuum prior to analysis. The Brunauer-Emmett-Teller (BET) method was applied to calculate the surface area, and the pore size distribution was obtained using the Barrett-Joyner-Halenda (BJH) and density functional theory (DFT) models.

2.4. Electrochemical Measurements

The electrochemical performance of the ZSCFC electrodes was evaluated using an electrochemical workstation (CHI 660E, CH Instruments, USA) in a three-electrode configuration and a symmetric two-electrode cell. 6 M KOH aqueous solution was used as the electrolyte for all tests. For the three-electrode system, the working electrode was prepared by mixing 80 wt% ZSCFC, 10 wt% carbon black, and 10 wt% PVDF

in NMP to form a slurry. The slurry was coated onto nickel foam and dried at 80 ℃ for 12 h. A platinum plate and Ag/AgCl electrode served as the counter and reference electrodes, respectively. Cyclic voltammetry (CV) was conducted at scan rates from 5 to 100 mV s^{-1} within a potential window of −1.0 to 0 V. Galvanostatic charge-discharge (GCD) tests were performed at current densities ranging from 0.5 to 20 A g^{-1}. Electrochemical impedance spectroscopy (EIS) was recorded from 100 kHz to 0.01 Hz with an AC amplitude of 5 mV at open circuit potential. For practical evaluation, symmetric supercapacitors were assembled using two identical ZSCFC electrodes separated by a cellulose filter paper. CV, GCD, and long-term cycling stability were measured at room temperature. The cycling performance was tested at 5 A g^{-1} for 10,000 cycles using a battery testing system (CT-4008T, Neware, China). Specific capacitance (C_s, F g^{-1}), energy density (E, Wh kg^{-1}), and power density (P, W kg^{-1}) were calculated from the GCD curves using standard equations.

3. Results and Discussion

3.1. Formation Mechanism of ZSCFC Porous Carbon

The preparation involves two main stages: carbonization and chemical activation. During the initial carbonization at 600 ℃, the lignocellulosic components of Z. spina-christi fruit decompose, releasing volatile compounds and forming a carbonaceous char with a preliminary porous framework. This char retains the natural fibrous structure of the biomass, which serves as a template for further pore development. In the subsequent activation stage, KOH or NaOH reacts with carbon at 800 ℃ through redox reactions such as $6KOH + 2C \rightarrow 2K + 3H_2 + 2K_2CO_3$. These reactions etch the carbon matrix, create micropores, and widen existing pores. The activation time plays a critical role in controlling porosity. At 2 h, moderate etching produces micropores that contribute to high surface area. Extending the time to 3 h promotes further pore development and interconnection, resulting in a hierarchical micro-mesoporous structure that facilitates faster ion diffusion. KOH generally exhibits stronger activation ability than NaOH due to the larger ionic radius of K^+, which enables more effective intercalation between carbon layers. Consequently, ZSCFC-3h-KOH developed the most extensive pore network and the highest specific surface area among all samples.

3.2. Morphology and Structure Characterization

The surface morphology and microstructure of the ZSCFC samples were examined using FE-SEM as shown in Figure 1. The raw Z. spina-christi char without activation exhibited a dense and blocky structure with limited porosity. After KOH activation for 2 h, ZSCFC-2h-KOH developed a loosely interconnected framework with abundant micropores distributed on the carbon surface, Figure 1A. Extending the activation time to 3 h for ZSCFC-3h-KOH led to a more open and hierarchical porous network composed of thin carbon nanosheets with well-defined mesopores, Figure 1B. This morphology provides abundant ion-accessible channels and reduces diffusion resistance. In comparison, NaOH-activated samples showed less developed porosity. However, ZSCFC-2h-NaOH displayed a compact surface with fewer pores, Figure 1C, while ZSCFC-3h-NaOH showed moderate pore formation but the pore walls remained thicker than those in KOH-activated carbons, Figure 1D. The difference arises from the stronger etching and intercalation ability of K^+ compared to Na^+ during activation.

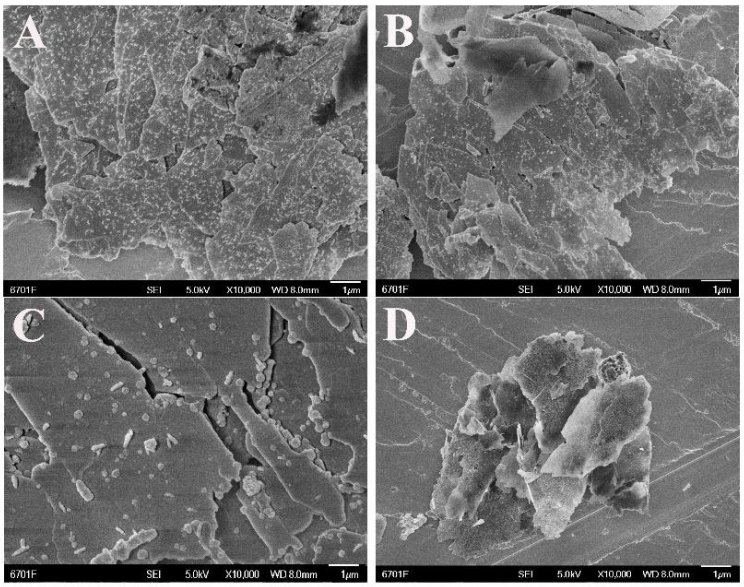

Figure 1. *FE-SEM images of (A) ZSCFC-3h-KOH; (B) ZSCFC-2h-KOH; (C) ZSCFC-3h-NaOH; and (D) ZSCFC-2h-NaOH.*

The crystalline structure was analyzed by XRD, Figure 2. All ZSCFC samples exhibited two broad diffraction peaks at $2\theta \approx 23°$ and 43°, corresponding to the (002) and (100) planes of disordered graphitic carbon. The (002) peak of KOH-activated samples shifted to lower angles compared to NaOH-activated ones, indicating a larger interlayer spacing. This expansion is attributed to the insertion of potassium species between carbon layers during activation, which creates more space for ion intercalation.

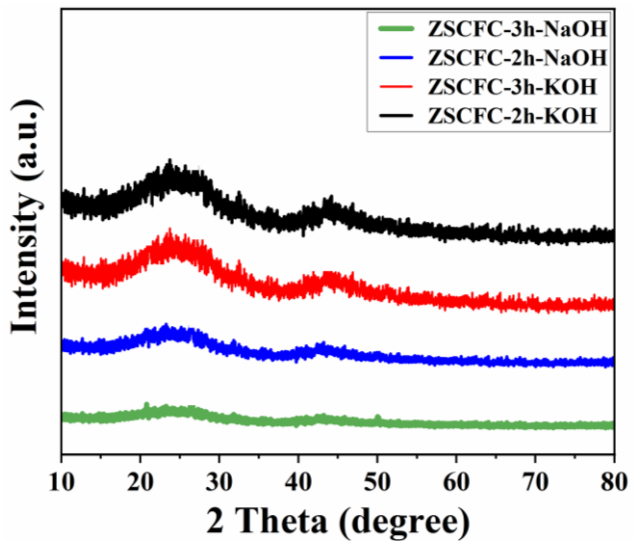

Figure 2. *XRD patterns of ZSCFC-3h-KOH; ZSCFC-2h-KOH; ZSCFC-3h-NaOH; and ZSCFC-2h-NaOH.*

Raman spectra, Figure 3, showed D and G bands at ~1340 cm^{-1} and 1590 cm^{-1} for all samples. The ID/IG ratio of ZSCFC-3h-KOH was 0.98, lower than that of ZSCFC-2h-KOH (1.00), ZSCFC-3h-NaOH (1.01), and ZSCFC-2h-NaOH (0.99). A lower ID/IG ratio suggests higher graphitization and improved electrical conductivity, which benefits charge transfer in supercapacitors. The porous texture was evaluated by N_2 adsorption-desorption isotherms. All samples displayed Type-IV isotherms with H4 hysteresis loops, confirming the coexistence of micropores and mesopores. ZSCFC-3h-KOH showed the highest nitrogen uptake and the most pronounced hysteresis at $P/P_0 > 0.4$, indicating a well-developed mesoporous structure. The pore size distribution, revealed that ZSCFC-3h-KOH possessed the largest pore volume centered around 2-4 nm.

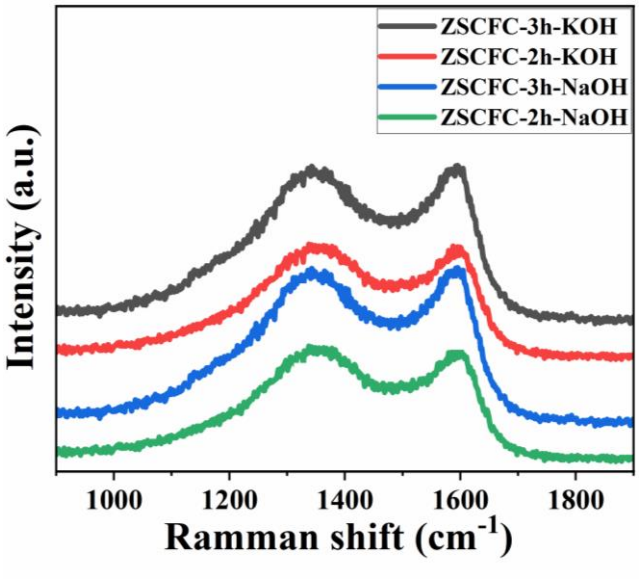

Figure 3. *Raman spectrum of ZSCFC-3h-KOH; ZSCFC-2h-KOH; ZSCFC-3h-NaOH; and ZSCFC-2h-NaOH.*

As summarized in Table 1, ZSCFC-3h-KOH achieved the highest specific surface area of 917.5 $m^2\ g^{-1}$ and the largest total pore volume. ZSCFC-2h-KOH reached 789.21 $m^2\ g^{-1}$, while NaOH-activated samples showed lower values of 696.18 $m^2\ g^{-1}$ and 674.55 $m^2\ g^{-1}$ for 3 h and 2 h, respectively. These results demonstrate that both of the activation agent and duration significantly affect the porosity. The optimal combination of KOH and 3 h activation produced a hierarchical pore structure with maximum surface area, which is expected to enhance the capacitive performance.

Table 1. *BET surface area, and pore structure characterization parameters of the different samples.*

Sample	S_{BET} ($m^2\ g^{-1}$)	d (nm)
ZSCFC-3h-KOH	917.5	3.68
ZSCFC-2h-KOH	789.21	3.12
ZSCFC-3h-NaOH	696.18	2.91
ZSCFC-2h-NaOH	674.55	3.02

[a]where: S_{BET}≡ specic surface area determined according to the BET method. d≡ adsorption average pore diameter.

3.3. The Electrochemical Performance

The capacitive behavior of the ZSCFC electrodes was first evaluated in a three-electrode system using 6 M KOH electrolyte. Figure 4A presents the CV curves of all samples at 20 mV s^{-1} within −1.0 to 0 V. All electrodes displayed a nearly rectangular shape without redox peaks, indicating typical electric double-layer capacitance behavior. Among them, ZSCFC-3h-KOH showed the largest enclosed area, reflecting superior charge storage ability. This improvement is attributed to its hierarchical porous structure and highest surface area. The cyclic voltammetry (CV) curves of the optimal ZSCFC-3h-KOH electrode, Figure 4B, maintained a quasi-rectangular shape even at high scan rates from 5 to 50 mV s^{-1}. The minimal distortion at 50 mV s^{-1} confirms rapid ion diffusion and excellent rate capability, consistent with its hierarchical porous structure. The GCD curves, Figure 4C, showed nearly symmetrical triangular profiles for all electrodes, indicating good capacitive behavior. Notably, ZSCFC-3h-KOH exhibited the most linear charge/discharge profile with a minimal IR drop of only 0.03 V, confirming superior reversibility, fast ion transport, and the lowest internal resistance among the series. The discharge time followed the order: ZSCFC-3h-KOH > ZSCFC-2h-KOH > ZSCFC-3h-NaOH > ZSCFC-2h-NaOH, which matches the trend of surface area. Calculated from GCD, ZSCFC-3h-KOH delivered a specific capacitance of 231.6 F g^{-1} at 1 A g^{-1}, significantly higher than ZSCFC-2h-KOH (177.9 F g^{-1}), ZSCFC-3h-NaOH (140.76 F g^{-1}), and ZSCFC-2h-NaOH (120.16 F g^{-1}), Figure 4D.

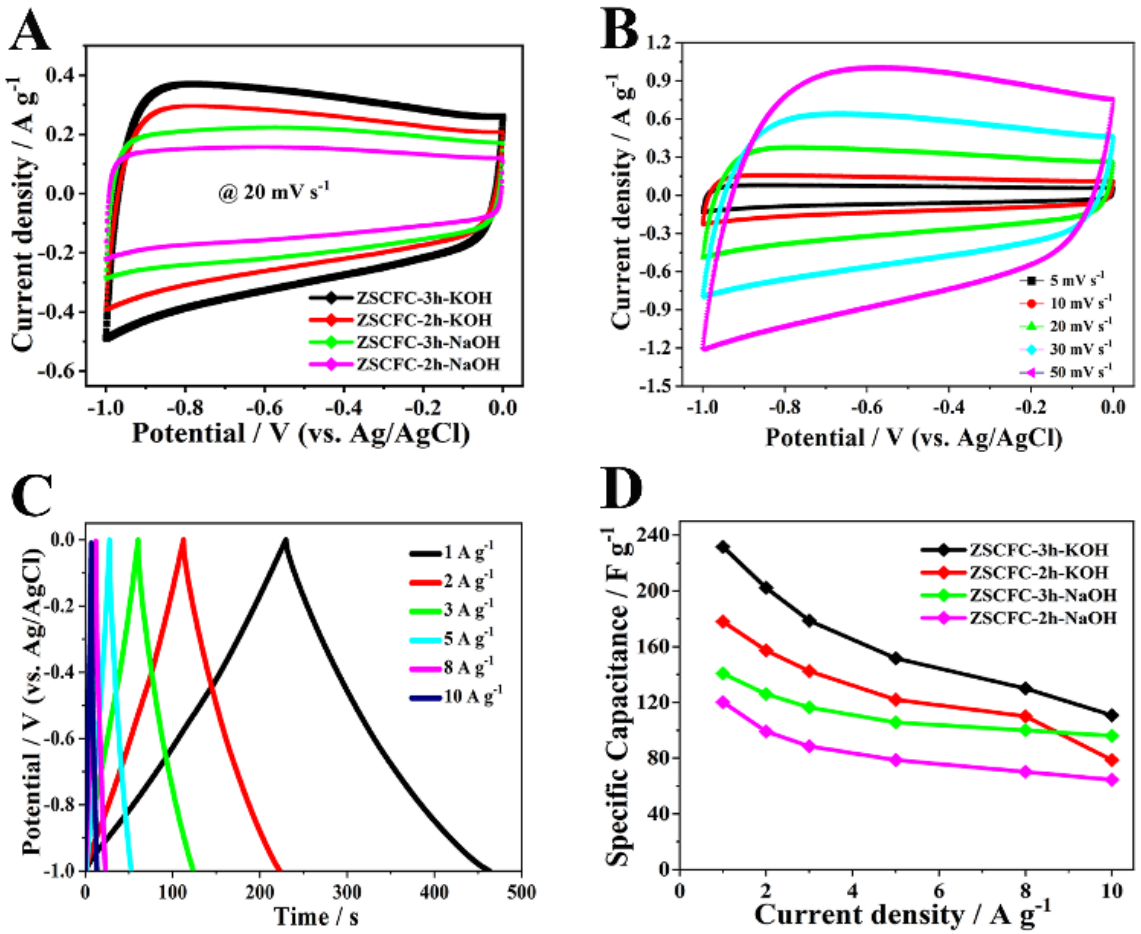

Figure 4. *(A) CV curves of ZSCFC-3h-KOH; ZSCFC-2h-KOH; ZSCFC-3h-NaOH; and ZSCFC-2h-NaOH at 20 mV/s; (B) CV curves of ZSCFC-3h-KOH; (C) curves of the GCD curves of ZSCFC-3h-KOH at different current densities; (D) Specific capacities of the ZSCFC-3h-KOH; ZSCFC-2h-KOH; ZSCFC-3h-NaOH; and ZSCFC-2h-NaOH electrodes at different current densities.*

Long-term cycling stability is critical for supercapacitors. Figure 5 shows that, the ZSCFC-3h-KOH electrode retained 94.3% of its initial capacitance after 10,000 charge-discharge cycles at 5 A g^{-1}. The minimal capacitance loss confirms the structural stability of the carbon framework and the absence of side reactions during cycling. Overall, the electrochemical results demonstrate that KOH activation for 3 h effectively optimizes the pore structure and surface chemistry of Z. spinachristi-derived carbon, thus, leading to high capacitance, excellent rate performance, and outstanding cycling stability.

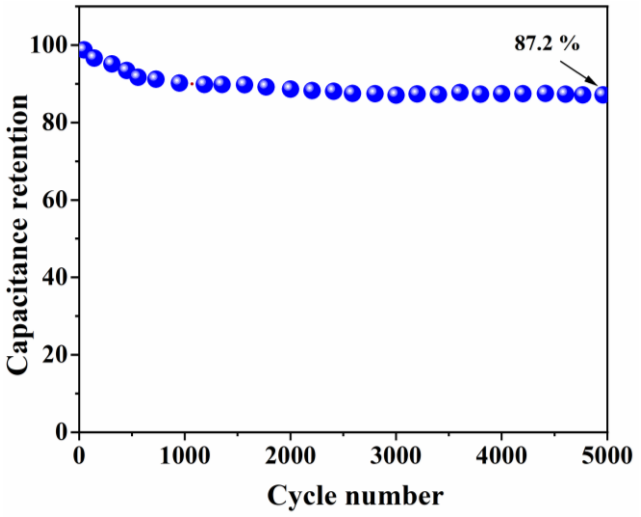

Figure 5. *Capacitance retention of ZSCFC-3h-KOH electrode over 5000 cycles.*

4. Conclusions

In summary, hierarchical N,O-doped porous carbon was successfully synthesized from Ziziphus spina-christi fruit waste using KOH activation at 3 h. The optimized ZSCFC-3h-KOH exhibited a high surface area of 917.5 m^2 g^{-1}, amorphous structure with abundant defects, and rough morphology. In a three-electrode system, it delivered a high specific capacitance of 231.6 F g^{-1} at 1 A g^{-1} and retained 96% capacitance after 5000 cycles. This work demonstrates that agricultural waste-derived carbon offers a sustainable and cost-effective electrode material for high-capacitance energy storage. In the future work we will focus on the fabricating symmetric supercapacitor devices to evaluate energy and power density.

Abbreviations

BET	Brunauer-Emmett-Teller
BJH	Barrett-Joyner-Halenda
CV	Cyclic Voltammetry
DFT	Density Functional Theory
EIS	Electrochemical Impedance Spectroscopy
FE-SEM	Field-Emission Scanning Electron Microscopy
GCD	Galvanostatic Charge-Discharge
PVDF	Polyvinylidene Fluoride
RHA	Rice Husk Ash
TEM	Transmission Electron Microscopy
XRD	X-ray Diffraction

Author Contributions

Hamouda Adam Hamouda: Methodology, Resources, Software, Writing – original draft

Inaam Ali Salim: Formal Analysis, Funding acquisition

Abdelwahab Abuelgasim Mohammed Adam: Conceptualization, Investigation

Taysir Abdrhman Musa: Formal Analysis, Validation

Elsadig Omer Fadul: Visualization, Writing – review & editing

Conflicts of Interest

The authors declare no conflicts of interest.

References

[1] Y. Li, Q. Lu, J. Yang, W. He, Delignified wood for thermal energy storage with high efficient photo-thermal conversion efficiency, Journal of Energy Storage, 80 (2024) 110235. https://doi.org/10.1016/j.est.2023.110235

[2] K. Sharma, S. Grover, P. Kadyan, S. Sharma, N. Kumar, R. K. Sharma, Synergistic effect of nitrogen and oxygen self-doping in bio-waste derived activated carbon for supercapacitor applications, Journal of Physics and Chemistry of Solids, (2025) 113471. https://doi.org/10.1016/j.jpcs.2025.113471

[3] N. M. Manousakis, P. S. Karagiannopoulos, G. J. Tsekouras, F. D. Kanellos, Integration of renewable energy and electric vehicles in power systems: a review, Processes, 11 (2023) 1544. https://doi.org/10.3390/pr11051544

[4] J. Wang, S. Kaskel, KOH activation of carbon-based materials for energy storage, Journal of materials chemistry, 22 (2012) 23710-23725. https://doi.org/10.1039/c2jm34066f

[5] E. C. Edwards, A. Holcombe, S. Brown, E. Ransley, M. Hann, D. Greaves, Evolution of floating offshore wind platforms: A review of at-sea devices, Renewable and Sustainable Energy Reviews, 183 (2023) 113416. https://doi.org/10.1016/j.rser.2023.113416

[6] M. D. Ahmed, K. M. Maraz, Revolutionizing energy storage: Overcoming challenges and unleashing the potential of next generation Lithium-ion battery technology, Materials Engineering Research, 5 (2023) 265-278. https://doi.org/10.25082/MER.2023.01.003

[7] D. Wang, Y. Hu, Z. Cui, P. Yang, Z. Du, Y. Hou, P. Yang, J. Rao, C. Wang, Y. Zhang, Sulfur vacancy regulation and multi-polarization of NixCo1S nanowires-decorated biotemplated structures to promote microwave absorption, Journal of Colloid and Interface Science, 646 (2023) 991-1001. https://doi.org/10.1016/j.jcis.2023.05.112

[8] W. Song, M. Yuan, K. Wang, X. Lian, H. Niu, Flexible N, S-co-doped hollow porous carbon film for high-rate and long-cycle supercapacitors, Chemical Engineering Journal, 516 (2025) 163970. https://doi.org/10.1016/j.cej.2025.163970

[9] Y. Zhao, J. Mu, Y. Wang, Y. Liu, H. Wang, H. Song, Preparation of hierarchical porous carbon through one-step KOH activation of coconut shell biomass for high-performance supercapacitor, Journal of Materials Science: Materials in Electronics, 34 (2023) 527. https://doi.org/10.21203/rs.3.rs-1895857/v1

[10] R. Chakraborty, K. Vilya, M. Pradhan, A. K. Nayak, Recent advancement of biomass-derived porous carbon based materials for energy and environmental remediation applications, Journal of Materials Chemistry A, 10 (2022) 6965-7005. https://doi.org/10.1039/d1ta10269a

[11] A. Khan, A. Patra, D. Chaira, D. A. Babu, B. Majumdar, Study of microstructure, thermodynamic and powder properties of nano Y_2O_3, TiO_2, ZrO_2 dispersed W-Ni-Nb-Mo-Zr alloys, Materials Chemistry and Physics, 311 (2024) 128567. https://doi.org/10.1016/j.matchemphys.2023.128567

[12] S. Joseph, G. Saianand, M. R. Benzigar, K. Ramadass, G. Singh, A. I. Gopalan, J. H. Yang, T. Mori, A. a. H. Al-Muhtaseb, J. Yi, Recent advances in functionalized nanoporous carbons derived from waste resources and their applications in energy and environment, Advanced Sustainable Systems, 5 (2021) 2000169. https://doi.org/10.1002/adsu.202000169

[13] T. Manimekala, R. Sivasubramanian, M. A. Dar, G. Dharmalingam, Crafting the architecture of biomass-derived activated carbon via electrochemical insights for supercapacitors: a review, RSC advances, 15 (2025) 2490-2522. https://doi.org/10.1039/d4ra07682f

[14] T. Khandaker, T. Islam, A. Nandi, M. A. A. M. Anik, M. S. Hossain, M. K. Hasan, M. S. Hossain, Biomass-derived carbon materials for sustainable energy applications: a comprehensive review, Sustainable Energy & Fuels, 9 (2025) 693-723. https://doi.org/10.1039/d4se01393j

[15] M. A. Abubakera, H. A. Hamouda, L. Chena, L. Dinga, S. Y. Zhua, L. W. Fua, J. Zhanga, Characterization of chemical structure of water-soluble polysaccharides from Sudanese Ziziphus spina christi fruits, Eurasian Chem. Commun, 3(2021): 200-209. https://doi.org/10.22034/ecc.2021.273357.1139

[16] R. Fennouh, O. Benturki, A. Mokhati, A. Benturki, B. Belhamdi, M. Trari, Preparation and characterization of highly mesoporous activated carbon from Ziziphus Spina-Christi for tartrazine adsorption from a simulated effluent, Biomass Conversion and Biorefinery, 14 (2024) 16171-16187. https://doi.org/10.1007/s13399-023-04458-9

[17] G. Simoes dos Reis, C. Mayandi Subramaniyam, A. D. Cárdenas, S. H. Larsson, M. Thyrel, U. Lassi, F. Garcia-Alvarado, Facile synthesis of sustainable activated biochars with different pore structures as efficient additive-carbon-free anodes for lithium-and sodium-ion batteries, ACS omega, 7 (2022) 42570-42581. https://pubs.acs.org/doi/10.1021/acsomega.2c06054

[18] E. Valsami-Jones, G. Chen, Abstracts of the 5th International Online Conference on Nanomaterials, in, MDPI, 2026. https://doi.org/10.3390/materproc2025025025

[19] A. M. H. Putri, B. F. Ramadhoni, Yuliusman, M. A. M. Yuzir, Y. Muharam, Activated carbon from tea twig waste via low-temperature KOH activation for efficient CO_2 capture: Development mesoporous structures under mild conditions, Adsorption Science & Technology, 43 (2025) 02636174251383610. https://doi.org/10.3390/materproc2025025025

[20] A. Ramadan, H. A. Hamouda, X. Zhu, J. Ding, H. Pei, N. Liu, R. Guo, Z. Mo, Fabrication of $Co_2Mn_3O_8$@ NiMnLDH nanocomposite array on nickel foam for oxygen evaluation reaction, Inorganic Chemistry Communications, 152 (2023) 110670. https://doi.org/10.1016/j.inoche.2023.110670

[21] H. A. Hamouda, S. Cui, X. Dai, L. Xiao, X. Xie, H. Peng, G. Ma, Synthesis of porous carbon material based on biomass derived from hibiscus sabdariffa fruits as active electrodes for high-performance symmetric supercapacitors, RSC advances, 11 (2021) 354-363. https://doi.org/10.1039/d0ra09509e